Low-field MRI can be more sensitive than high-field MRI

Aaron M. Coffey[1, 2], Milton Truong,[1] and Eduard Y. Chekmenev*[,1,2,3]

[1]Department of Radiology, Vanderbilt University Institute of Imaging Science (VUIIS), Nashville, Tennessee, 37232, United States

[2]Department of Biomedical Engineering, Vanderbilt University, Nashville, Tennessee, 37235, United States

[3]Department of Biochemistry, Vanderbilt University, Nashville, Tennessee, 37205, United States

*Correspondence to: eduard.chekmenev@vanderbilt.edu

Supplementary Materials

Equation (S11-S21)

Figure S4

Table (S1-S6)

Theory

1. Litz wire calculations
2. Equations for deriving sample resistance percentage

Materials and Methods

1. MRI scanner systems
2. Inductive detection of the multi-turn solenoidal RF coil

    2a. The use of Litz wire

    2b. Series vs. parallel solenoid wind

    2c. Balancing number of turns, proximity effect, and crystal radio coils

    2d. Multi-layered solenoids
3. Experimental limitations and their SNR correction factors

    3a. Coil coupling losses

    3b. Increase of 4.7 T $R_S T_S$ term

    3c. Stranding gauge effect

    3d. Proximity effect calculation

Theory

1. Litz wire calculations

Proximity effect losses rather than skin effect losses are known to dominate in multi-stranded, multi-turn coils. *Litzendraht* or Litz wire, a woven form of stranded wire, is commonly used to mitigate skin and proximity losses relative to solid wire in high-frequency transformer windings. The significant minimizations of these losses lead to prior use in RF coils at low B_0 field [1, 2] strengths. In principle, the woven strands undergo radial and azimuthal transposition to force the condition that every strand occupies the space of every other strand in the wire so that the overall magnetic field acts equally on all strands. The equal application results in uniform current distribution thereby minimizing high-frequency resistance [3].

The resistance reduction of Litz over the equivalent solid wire has an analytical form reproduced here for completeness. Using the derivations of Lotfi [3], Litz wire losses can be assessed and the proper wire selected for the detection frequency ω_0. The effective series resistance (ESR) of a Litz wire is the sum of the proximity effect losses R_e and the skin losses R_{skin}, or $R_{Litz} = R_e + R_{skin}$. The proximity effect losses are evaluated as [3]

$$R_e = \frac{p}{2\pi\sigma r_{st}^2}\frac{r_{st}}{\delta}\frac{\mathrm{Re}\left[(1-j)I_0(kr_{st})I_1^*(kr_{st})\right]}{\left|I_0(kr_{st})\right|^2} \tag{S11}$$

where δ is the skin depth, $k = (1+j)/\delta$ is the complex wave number, the imaginary number $j = \sqrt{-1}$, σ is the conductor conductivity, I_0 and I_1 are modified Bessel functions of the first kind where I_1^* is the complex conjugate, and p is the packing factor given by

$$p = S(r_{st}/r_b)^2 \tag{S12}$$

for a wire bundle of radius r_b with S strands of radius r_{st}. Similarly, skin effect losses are expressed as [3]

$$R_{skin} = \frac{1}{2\pi\sigma S r_{st}\delta}\mathrm{Re}\left[(1+j)\frac{I_0(kr_{st})}{I_1(kr_{st})}\right]. \tag{S13}$$

The resistance R_{solid} of the equivalent solid wire with a smaller radius $r_s = r_b\sqrt{p}$, is found using [3]

$$R_{solid} = \frac{r_b\sqrt{p}}{2\delta}\mathrm{Re}\left[(1+j)\frac{I_0\left(\frac{r_b\sqrt{p}}{\delta}\right)}{I_1\left(\frac{r_b\sqrt{p}}{\delta}\right)}\right]. \tag{S14}$$

Using Eqs. (S11 – S14), a frequency dependent resistance reduction factor is defined [3], or

$$\eta_{Litz} = R_{Litz} / R_{solid}, \tag{S15}$$

yielding an optimum frequency f_0 at the minimum of η_{Litz}. With ideal wire selection, $f_0 = \omega_0$ and η_{Litz} is the global minimum.

2. Equations for deriving sample resistance percentage

Sample resistance relative to coil resistance is typically ascertained from coil loading factor measurements due to the simplicity of measuring coil Q when loaded by the sample and coil Q when unloaded. The equation given by Gilbert relating loading factor L_F, Q measurements, and the resistances [4] is

$$L_F = 1 - \frac{Q_L}{Q_U} = 1 - \frac{R_C}{R_C + R_S}. \tag{S16}$$

After algebraic manipulation of Eq. (S16), sample resistance R_S may be expressed as a percentage of coil resistance R_C as

$$R_S = \left[\left(\frac{Q_L}{Q_U} \right) - \left(\frac{Q_L}{Q_U} \right)^2 \right] R_C \,. \tag{S17}$$

The sample resistance R_S may also be derived from peak-to-peak noise measurements from the RF coil in the MRI scanner after a $\tau_{90°}$ square excitation RF pulse with (N_S+N_C) and without sample present (N_C). As the resistances related by Eq. (S17) are defined by a Q measurement ratio, R_S and R_C may be similarly separated and expressed as relative percentages based on a noise measurement ratio. With $Q_L/Q_U < 1$, one may similarly equate the noise measurements to reflect an analogous ratio defined as $N_C/(N_S + N_C) \equiv Q_L/Q_U$ for sample noise N_S and coil noise N_C. Consequently, sample resistance may also be expressed as a percentage of coil resistance as

$$R_S = \left[\left(\frac{N_C}{N_S + N_C} \right) - \left(\frac{N_C}{N_S + N_C} \right)^2 \right] R_C \,. \tag{S18}$$

The noise measurements are inclusive of the preamplifier noise figure F, Eq. (S1), at the detection frequency ω_0, and it cancels in the above ratio negating its effect on this calculation.

Materials and methods

1. Sample phantoms and preparation of nuclear spin polarizations significantly exceeding thermal level (prepolarization)

^{1}H and ^{13}C spectroscopic and imaging comparisons utilized two spherical phantoms of sodium 1-^{13}C-acetate. The phantom for ^{1}H studies was 1.0 g of sodium 1-^{13}C-acetate (Isotec-Sigma-Aldrich) dissolved in 99.8% D_2O resulting in 2.8 mL total volume. A larger sample for ^{13}C studies consisted of 5.18 g of sodium 1-^{13}C-acetate dissolved in 99.8% D_2O resulting in 17.5

mL total volume. High-field data were acquired on a 4.7 T Varian small animal MRI scanner with a multi-nuclear RF probe (Doty Scientific, Columbia, SC). Low-field data were collected on a 0.0475 T spectrometer (Magritek, Wellington, New Zealand) equipped with a gradient coil insert (Magritek) and in-house developed H-X and X-H RF probes, where the X channel was tuned and optimized to the ^{13}C resonance frequency.

Prior to spectroscopic or MR imaging at 0.0475 T as shown in Figs. 1 and 2, the sample was prepolarized, i.e. its nuclear spin polarization P was enhanced significantly above its equilibrium level at 0.0475 T. For ^{1}H studies, the sample was prepolarized at 9.4 T for > 30 seconds, and detection at 0.0475 T occurred following an ~5 second transfer delay. At detection, the resulting ^{1}H polarization was $P = (1.050\pm0.016)*10^{-5}$. Polarization level was calculated by comparison of the prepolarized NMR signal intensity with that of the thermally polarized sample. Similarly for ^{13}C studies, the sample was prepolarized at 7.0 T for > 5 minutes, and detected at 0.0475 T following an ~5 second transfer delay. ^{13}C polarization was calculated as $P = (4.70\pm0.02)*10^{-6}$ by again comparing prepolarized NMR signal intensity with that of the thermally polarized sample.

Spectroscopic results (Fig. 2) used identical acquisition parameters on the two MRI systems: square RF excitation pulses with calibrated $\tau_{90°}$, 1 k complex acquisition points, spectral width of 2 kHz, and 500 ms acquisition time. Imaging (Fig. 1) was similarly performed with identical parameters with the exception of ^{13}C RF excitation pulse angle α. On the 4.7 T scanner, images were acquired with Varian's 2D balanced FSSFP sequence. At 0.0475 T, Magritek's fast 2D gradient echo sequence was used. For ^{1}H on both systems RF excitation pulse angle $\alpha = 18°$, spectral width was 10 kHz, and acquisition time was 6.4 ms per line of k-space. ^{13}C imaging parameters were spectral width of 5 kHz, 6.4 ms acquisition time, pulse angle $\alpha = 90°$ at 4.7 T,

and $\alpha = 18°$ at 0.0475 T. For the latter the reduced angle was necessary to avoid consuming too much polarization during gradient echo imaging acquisition of k-space. ^{1}H imaging in-plane resolution was 0.375×0.375 mm^2, (field of view = 24×24 mm^2), and ^{13}C was 2.5×2.5 mm^2 (field of view = 80×80 mm^2) respectively. The resulting ^{1}H and ^{13}C images with 64×64 and 32×32 imaging matrices and they are presented without any extrapolation or any further manipulation.

2. MRI scanner systems

The high-field preclinical Varian MR scanner (Fig. 3) used in this study was located in a shielded room. The system consisted of a gradient insert with a 120 mm inner diameter, a superconducting 4.7 T magnet including cryogens weighing approximately 3410 kg, and a multi-nuclear probe from Doty Scientific (Columbia, SC). The RF probe had a bore of 38 mm for small animal studies. The detection coil diameters measured were 44 mm for ^{1}H, 53 mm for ^{15}N and 61 mm for ^{13}C.

The low field MR scanner (Fig. S4) did not require a shielded room. The system consisted of a gradient insert (Magritek, Wellington New Zealand) with an 89 mm inner diameter, a 0.0475T permanent magnet Halbach array (Magritek, Wellington New Zealand) weighing 50 kg, and in-house multi-nuclear probes. The magnet was mounted on a wheeled cart with a transit mount to permit ease of transportation and switching between spectroscopic orientation (vertical) and MR imaging orientation (horizontal). The console consisted of a Kea2 spectrometer (Magritek, Wellington New Zealand) provided with narrow-band preamplifiers (Miteq, Hauppauge, NY), a custom RF amplifier with two 250 W channels (Tomco, Stepney, Australia), and gradient amplifiers (part 8205, AE Techron, Elkhart, Indiana). The gradient amplifiers were connected to the gradient coils via 10 AWG stranded wire (part number 71245K51, McMaster, Aurora, OH)

as a twisted pair for each axis and all contained in a braided copper mesh sleeve (part number 5537K28, McMaster, Aurora, OH). Toroidal RF chokes (part number ZW-44932-TC, Elna Magnetics, Saugerties, NY) were used to minimize gradient noise above the 100 kHz cut-off with the twisted pair wire forming 5 turns through two chokes per axis. A separate ground connection between magnet and console (part number 71245K55, McMaster, Aurora, OH) also used two of these RF chokes. To further reduce gradient noise, the gradient insert was lined with 0.127 mm copper foil (part number 9709K62, McMaster, Aurora, OH). Other than the probe RF shield PCB end plates, the magnet bore ends were otherwise open.

The 0.0475 T probes were constructed with geometry similar to the Doty probe. The H-X and X-H dual channel RF probes had an inner bore of 38 mm of the detection inner solenoid coil at a diameter of 42 mm and the outer RF excitation coil of the second channel at 51 mm. X channel was tuned to ^{13}C resonant frequency, but this broadband channel can be also tuned to ^{129}Xe and ^{23}Na resonant frequencies. The probe coils were constructed of Litz wire selected for the best experimentally determined strand gauge and strand number for the detection frequency ω_0 (Computer Controlled Automation Inc, Middletown, OH). The inner detection coil was optimized for the detection frequency ω_0 and together with the outer excitation coil was enclosed within an RF shield (Fig. S4B) of copper mesh (part number 9224T44, McMaster, Aurora, OH) and copper PCB end plates (part number PC11-T-ND, Digikey, Thief River Falls, MN). 50 Ω impedance, non-magnetic RG-405 coaxial cable connected the RF coils to BNC connectors in brass mounting plates. The capacitive tuning and matching network configurations for the probe coils were balanced RF circuits (Fig. S4A).

The balanced tuning and matching circuit [5] reduces potential losses. It provides electrical balancing and halves the voltage amplitude across the coil by putting a virtual ground at the coil

center consequently reducing dielectric losses. C_0 serves to pre-tune the coil and concentrates the current in the probe coil. The RF circuits were built in external RF isolated boxes (part number 501-1111-ND, Digikey, Thief River Falls, MN). The capacitance from the RG-405 and the BNC cables (part number ACX1789-ND, Digikey, Thief River Falls, MN) served to aid in pre-tuning the coils, albeit in other circumstances it may prove desirable to avoid the extra capacitance in order to increase the coil inductance L. The tuning and matching was achieved with fixed C22CF series capacitors (Dielectric Laboratories, Cazenovia, NY) used in parallel with variable capacitors (model NMTM120C / HSF250, Voltronics, Denville, NJ or model 5601, Johanson, Boonton, NJ). The component values for the RF probes and the RF coil τ_{90° pulse lengths using 200 mW of power are given in Table S1.

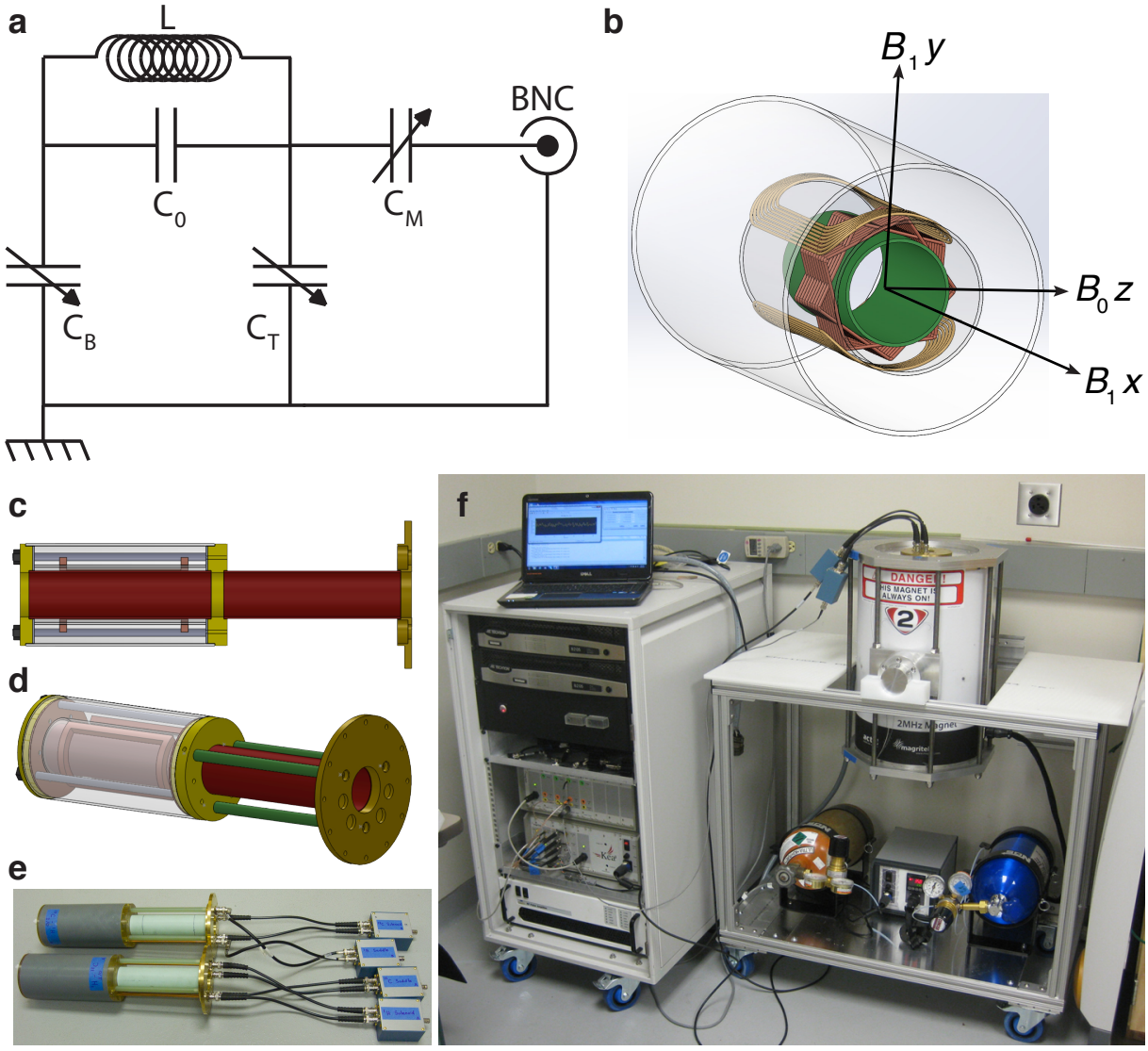

FIG. S4. The 0.0475 T MR scanner system. A) The balanced tuning/matching circuit; B) Representation of the inner basket weave $^{1}H/^{13}C$ detection coil, outer Helmholtz saddle coil for $^{13}C/^{1}H$ excitation, and RF shield support tube; C) and D) views of the 0.0475 T probe design; E) realization of the H-X and X-H probes with attached tuning/matching boxes; F) View of overall MR scanner system in the vertical spectrometer configuration.

Table S1. RF circuit (Fig. S4A) component values and performance measures.

Probe	Channel	Capacitor	Capacitor Value (pF)	Litz Wire	Number of turns	Q	L (μH)	$\tau_{90°}$ (μs) / 200 mW	B_1 (kHz) / 200 mW
H-X, X=^{13}C	^{1}H	C_0	15	175/ 46	64	62	112.2	76	13.2
		C_T	1 - 30, 51						
		C_B	1 - 30						
		C_M	0 - 120, 68						
	^{13}C	C_0	579	60/ 44	26	50	152	400	2.5
		C_T	1 - 30, 304						
		C_B	1 - 30, 180						
		C_M	0 - 120, 610						
X-H, X=^{13}C	^{13}C	C_0	100	20/ 44	132	28	425	206	4.9
		C_T	0 - 120, 100						
		C_B	0 - 250						
		C_M	2 - 250, 1800						
	^{1}H	C_0	131	175/ 46	14	96	52.4	141	7.1
		C_T	1 - 30						
		C_B	1 - 30						
		C_M	0 - 120, 151						

2. Inductive detection of the multi-turn solenoidal RF coil

The volume coil with the greatest detection sensitivity is the solenoidal coil [6]. The design variables for solenoid SNR are the detection frequency ω_0, coil sensitivity according to B_1, and total effective series resistance of the noise sources [7]. Analytically, the solenoid has 3.09 times greater SNR compared to a saddle coil [6] owing to greater efficiencies in B_1 and reduced coil resistance R_C due to more efficient use of wire to form turns. The maximum SNR for a solenoid is attained when its length to diameter ratio is between 0.7 and 0.8 [8, 9]. However, higher SNR does not coincide with better B_1 homogeneity, important for uniform RF excitation of the sample, as the two properties are mutually exclusive [10]. Optimum coil design therefore entails establishing a balance between the two.

The dominant noise sources in MR are coil noise, sample inductive losses, and sample dielectric losses. Many sources in the literature [1, 4, 6, 8, 9, 11, 12] have noted the proportionality of coil noise to $\omega_0^{1/2}$, sample inductive losses to ω_0^2, and sample dielectric losses to ω_0^3 [6] or, in a more developed model [13] later extended [14], to ω_0^4. As a result, the sample associated losses, or body noise, degrade coil sensitivity at higher frequency ω_0 [4].

The coil sensitivity can be divided into two operating regimes based upon the changing dominance of the noise sources scaling with ω_0. A transition point between the two occurs when the sample losses become equal to the coil losses, after which body noise is said to dominate the coil sensitivity; e.g., for human head sized samples this point is below 8.2 MHz [9]. Work by Gilbert [4] measured the coil sensitivity degradation through loss of coil quality factor Q through the transition from the coil noise to body noise dominated regime. As $SNR \propto \sqrt{Q}$ [9], there is no practical benefit of going to detection frequencies higher than the coil noise dominated regime

[1, 4] for polarization P endowed by hyperpolarization. The factor Q can be modified by proximity of the RF coil to the surrounding shield [6] to reduce external noise. Detection below the transition point in the coil noise dominated regime implies three areas of improvement: (i) increasing the detection frequency, (ii) increasing the RF shield diameter, (iii) decreasing the effective resistance R_C of the RF coil [4]. Consequently, strategies for optimizing RF coils using lossy conductors in the coil noise dominated SNR regime Eq. (S8) therefore revolve around fitting the coil very closely around the anatomy of interest [11], raising the detection frequency to the maximum level concomitant with the application, and minimizing R_C subject to the restriction that coil geometry permits fitting the length of wire allowed by the frequency.

RF coil efficiencies can be compared by several NMR spectroscopic measures when a square RF pulse at a fixed power setting is used to excite an identical sample. The detected SNR of the sample is maximal when the transmitted RF pulse length is calibrated to yield a 90° excitation. By reciprocity, transmit efficiency also measures detection sensitivity with both corresponding to the B_1 efficiency of the coil with regards to coil resistance R_C, or $SNR \propto B_1 / \sqrt{R_C}$ [6]. Additionally, the product of R_C and the proximity effect ζ can be evaluated by Eq. (S1) subject to preamplifier noise figure F by measuring the peak-to-peak noise voltage, $N_S + N_C$. These measures and integrated NMR signal together with the coil parameters such as self-resonance frequency (SRF) are given in Table S2 and constitute the means of evaluating the RF coil designs tested. Measurements were taken with an Agilent 4263B LCR meter with a 16334A test fixture at 100 Hz, with an Agilent E5071C network analyzer using a compensated cable, or with the 0.0475 T MRI scanner described above.

Table S2. Comparisons of detection coils tested in isolation (no saddle coil)

Coil Ref	Coil Type	Wire Type	Number of Turns	Length (mm)	Turns per mm	L (μH)	SRF (MHz)	Q Factor	$\tau_{90°}$ (μs)	Noise (μVp-p)	NMR Signal (a.u.)
A	Series	20 AWG	16	51.0	0.3	18.0	29.4	46.0	93	0.310	0.0534
B	Series	20 AWG	32	51.0	0.6	36.0	17.6	73.0	73	0.410	0.0682
C	Series	220/46	32	51.0	0.6	35.1	17.4	88.7	70	0.310	0.0737
D	Series	175/46	29	51.0	0.6	32.4	17.9	85.3	68	0.310	0.0745
E	Series	175/46	29	82.0	0.4	25.2	20.9	64.0	100	0.310	0.0482
F	Parallel	175/46	29 + 29	82.0	0.7	25.4	21.6	70.0	89	0.360	0.0572
G	Series	175/46	58	82.0	0.7	68.5	10.8	90.2	76	0.311	0.0603
H	'Basket'	175/46	64	53.0	1.2	112.2	7.7	97.3	64	0.280	0.0806

2a. The use of Litz wire

Wire selection is a complicated issue due to interaction with fixed coil volume. There is an inherent dilemma in the use of larger wire diameters [9], which can be seen from Eqs. (S1, S8, S10). As the wire diameter d_W increases, in order to maintain coil volume the coil diameter d_C must increase, which reduces B_1 and increases total conductor length leading to higher resistance, too. The consequence is reduced SNR.

Litz wire presents an opportunity to improve the SNR without increasing the wire diameter, which avoids the above conundrum. If solid wire and Litz wire forming two coils are of equal wire diameter and the turn spacing is identical, the proximity effect ζ acting upon the wires should also be identical. The skin effect Eq. (S6) leaves much of the conductor volume in a solid wire unused provided $d_W \gg \delta$, with the current J flowing through an annulus of width δ. Wire resistance R_C corresponds to the cross-sectional area A the current flows through, Eq. (S7). If we

define $\eta_{Litz} \equiv 1/\beta$ and $\beta > 1$ given $\eta_{Litz} < 1$, then the product $R_C \cdot \eta_{Litz} = \rho l/\beta A$, and so there is an increase in effective area βA commensurate with the reduction in resistance η_{Litz}. Effective diameter of the Litz wire expressive of this effective area may be defined then as $\beta A = 0.25\pi d_L^2$. Consequently, the resistance reduction compared to solid wire η_{Litz} may be analogously represented as an increase in effective Litz wire diameter d_{eff} according to

$$d_{eff} = \sqrt{\frac{4}{\pi}\beta A} = \beta^* \sqrt{A} \tag{S19}$$

where $\beta^* > 1$. Thus, Litz wire of the same diameter as a solid wire is anticipated to increase the SNR analogously as an apparent diameter increase provided $\eta_{Litz} < 1$. However, the solid wire with the conductor volume equivalent to the Litz wire bundle has a smaller radius $r_S = r_b\sqrt{p}$ [3] since packing factor $p < 1$ always. Thus Eq. (S19) provides a simple, convenient theoretical analogy for visualizing the reduction in resistance with Litz wire.

Litz wire [1-3, 15] has been used favorably to reduce coil resistance R_C at low frequencies. To ascertain its benefit in the 0.0475 T MR scanner probes, a coil (B, Table S2) was wound with 20 AWG magnet wire (part number 7588K81, McMaster, Aurora, OH), and a second coil (C, Table S2) of Litz wire consisting of 220 strands of 46 AWG wire (Computer Controlled Automation Inc., Middletown, OH). Ignoring packing factor p, the two coils were sufficiently equivalent for the purposes of this test, having the same wire diameter, turn spacing, and length. While $\sqrt{p} < 1$ means 20 AWG wire is better than the 220/46 Litz wire on the basis of its greater total conductor area, the proximity effect ζ was anticipated to act equally for the same turn spacing.

Coil measurements found the Litz wire more advantageous than solid wire for building coils with maximum detection sensitivity. For (B $\perp$ C) (B compared to C), the Litz coil had more

NMR signal at a lower measured noise level, yielding the anticipated improvement in $SNR \propto B_1 / \sqrt{R_C}$ [6]. This was also corroborated by the reduced τ_{90° pulse lengths. Together with the higher $Q = \omega_0 L / R_C$ despite slight decrease in Litz coil inductance L, the aforementioned measurements demonstrate $\eta_{Litz} \cdot \zeta \cdot R_C < \zeta \cdot R_C$, and $\eta_{Litz} < 1$ as expected.

2b. Series vs. parallel solenoid wind

Historically there has been need to reduce the inductance of a coil to better match the application. Commonly this goal is achieved by connecting the coil wires in parallel, as inductors conform to the same rules as resistors. Parallel coils have been mentioned in the context of NMR and MRI regarding favorable decrease of inductance [6] or resistance [2]. A parallel combination can also increase SNR [16] or mitigate λ/10 wire length restrictions. The former uniquely combines two adjacent coils whose wires are respectively wound clockwise and counterclockwise with no coil overlap. The outer pair of wires and the inner pair at the coil center are then connected together to form the parallel combination. Total coil inductance and resistance are both halved, which suits the coil application under specific circumstances.

There are two comparisons for parallel wound coils and series wound coils. For (E ⊥ F), two coils had essentially the same coil length, wire type, inductance, resistance, and self-resonance frequency. They differed in number of turns and proximity effect ζ with the latter's increase of effective series resistance for the parallel coil reflected in the Q measurement. Despite greater ζ due to decreased turn spacing, the parallel coil F demonstrated significant improvement in τ_{90° and minor improvement of SNR due to increased noise nearly commensurate with the NMR signal increase. The parallel coil represents an improvement. (F ⊥ G) examines the case of a series coil formed from the same length of wire as a parallel coil to compare coil winds with

identical number of turns and proximity effect factor but all other parameters differing. The series coil has less noise and demonstrates improvements in efficiency on the basis of both τ_{90° and NMR signal. However, it should be noted that the inductance increases greatly and the SRF correspondingly decreases for G compared to E and F. In this case, the series coil demonstrates better performance.

The question of what conditions favor a parallel coil over a series wound coil depends upon the winding restrictions in the context of available wire length. If a λ/10 wire length restriction causes the condition of too little available wire length, a parallel winding permits a larger number of turns and a more efficient coil (E ⊥ F). Too many turns, however, can also become a restriction as $L \propto n^2$ and $R_C \propto n$. While inductance L increases at a greater rate than the resistance leading to higher Q and hence coil sensitivity (F ⊥ G), the rapid increase in L with turns can lead to an inductance restriction at the resonant frequency $\omega_0 = \left[L\left(C_T + C_P\right) \right]^{-1/2}$ as parasitic capacitances C_P in the system can lead to achieving a proper tuning capacitance C_T untenable due to what is then overly large L. Under this condition, the parallel wind's reduced L becomes favorable and permits greater use of the available wire length.

In conclusion, turn-for-turn a series wind has better performance when wire length used to form the coil is constant and no inductive limit exists. A parallel wind can address the restrictions of an inductive restriction or a λ/10 wavelength restriction on the available wire length and consequently yield better performance than the series wind. The former restriction obtains in the case of small animal imaging coils, with the latter the case for large coils as for human imaging. A parallel wind is noisier, however, according to this test.

2c. Balancing number of turns, proximity effect, and crystal radio coils

Optimizing the RF coil entails maximizing $SNR \propto B_1 / \sqrt{\zeta R_C}$. B_1 improves linearly with number of turns, Eq. (S3), and thus conductor length, but greater conductor length increases coil resistance R_C and reduces the coil sensitivity. Nevertheless, both variables are linearly dependent on the number of turns n, and increase of n without other mitigating factors should lead to greater SNR. The proximity effect ζ also factors into the resistance, however, as a function of turn spacing and must be considered as part of the winding geometry. The proximity effect causes a reduction in the current-carrying cross-sectional area of the conductor due to proximity to nearby conductors thereby causing an increase in a coil's resistance. Proximity effect is maximal in the close wound condition of no turn spacing. However, even in this condition 15% SNR improvement for coils using Litz wire compared to wire spaced by one diameter has been demonstrated [1]. The proximity effect dependencies have been derived empirically for solid conductors by Medhurst [17], with wire diameter-to-turn spacing and coil length-to-coil diameter being the variables determining the proximity factor. Thus, improving SNR becomes a complex balance of number of turns and the proximity effect acting upon them in the context of the available space.

There are several ways of improving the SNR with regards to the above concerns. Whether the coil is solid wire for (A ⊥ B, Table S2) or Litz wire for (E ⊥ G), increasing the number of turns can improve the SNR until the limit imposed by the proximity effect is reached. The test (C ⊥ D) examined the impact of proximity effect by winding two coils identically except for wire selection. Fewer strands used in D and hence smaller wire diameter resulted in greater turn spacing and hence less proximity effect. Additionally, the use of fewer strands resulted in less strand-to-strand inductance which also lowered Q. Nevertheless, a reduced proximity effect

resulted in improved NMR signal for D despite loss of Q, and coil noise was measured as the same. (D ⊥ E) verified the expected loss of NMR signal due to less inductance of a solenoid when the turns are kept constant but the coil length is increased, mirrored in lower Q and thus coil sensitivity. Consequently, for a fixed coil length the SNR must be maximized by carefully balancing the confluence of number of turns, R_C according to wire diameter, and the proximity effect according to the turn spacing.

The maximization of SNR mentioned above is identical in formulation to the task of building the most efficient RF coil possible: a problem previously addressed in regards to crystal radio coils in the early years of radio. The coils had to possess high efficiency by maximizing Q. Two factors were critical in this application. Coil parasitic capacitance and proximity effect had to be minimized in order to have Q sufficient to extract enough power for listening and to permit station selection between the narrow bands. These factors were minimized through the use of unique coil winds that kept the turns well spaced in spite of a high turn density due to close winding, or diameter-to-turn spacing ratio (d/s) = 1. Of the various coil wind solutions devised such as the spiderweb or the honeycomb, the basket weave conforms most closely to the singly layered solenoid geometry.

A basket weave coil was constructed for comparison with the best performing classical solenoid, (D ⊥ H). It was constructed of 175/46 wire in accord with (C ⊥ D) wire test results and in favor of more turns. The basket weave's creation entailed passing the wire over and under nine 1.75 mm diameter, double-pointed, aluminum knitting needles evenly spaced around the 42 mm outer diameter coil tube (part number 6394A39, McMaster, Aurora, OH) until 64 turns were completed. The needles were removed after locking the wires in place with Sally Hansen Xtreme Wear #100 Invisible (sku number 693955, CVS, Woonsocket, RI) brand nail polish as a suitable

substitute for nitrocellulose-based coil dope. The choice of nine needles lead to approximately half the wire estimated as being in the close wound condition (d/s) = 1, and the other half with (d/s) = 0.5 with regards to proximity effect calculations from the Medhurst data. The potential of using more spacing elements during the coil winding to investigate proximity effect mitigation and SNR effects was not pursued. Nevertheless, with the close wound condition being the most unfavorable for proximity effect, it is suggested that more spacing elements be used when winding to ensure a greater percentage of the wire enters the (d/s) = 0.5 condition.

The basket weave outperformed the best solenoid coil. For (D ⊥ H), both the NMR signal and the noise for the basket weave H showed significant improvement. While $SNR \propto \sqrt{Q}$ only if B_1 and coil inductance L are maintained constant [1], examination of signal improvement from increased Q is still useful. The higher value of Q for H did not fully account for the greater signal, which was 0.0806 compared to 0.0796 projected from D according to $Signal \cdot \sqrt{Q_B/Q_S}$. We speculate that the higher turn density of the basket weave enhanced detection of the magnetic flux due to closer proximity of more turns to the sample, as such dipolar magnetic fields decay inversely with the cube of the distance. Lower noise was measured for the basket weave despite close winding of the wire, normally the condition for maximum proximity effect. Noise lower than the solenoid implies lower total effective resistance ζR_C than the solenoid despite a greater number of turns and their associated resistance. Consequently, the winding geometry of the basket weave, similar to the case with crystal radio coils, demonstrates a coil geometry benefit regarding proximity effect that exceeds the effect of the coil having 2.21 times the number of turns of the solenoid. Crystal radio coils were therefore found to be of benefit to MR on both the basis of signal and noise. To the best of our knowledge this work is the first report of using basket weave RF coils in magnetic resonance.

2d. Multi-layered solenoids

Faraday's law of electromagnetic induction states that the induced electromotive force $emf = -n \cdot d\Phi_B / dt$, the product of the number of turns *n* and the time derivative of the magnetic flux. This product was shown previously to permit nearly field independent NMR signal sensitivity without reference to noise [18]. An obvious method of obtaining more *emf* in the situation of fixed coil length is use of a multilayer coil design. However, it has been demonstrated for thick, single conductors that SNR does not improve with multilayers [19], an observation in accord with the theoretical model that SNR should decrease with increased layers for thick conductors [20]. Although written for solenoid microcoils, the premises of the model and the boundary conditions have validity for larger scale solenoids. This model also predicts that SNR improves with multilayers provided the conductor thickness is on the order of the skin depth, a situation which could obtain when Litz wire is used provided the improvement is applicable on the strand level rather than the Litz bundle level. The strand level premise was tested [2], but the second layer was found to be of no benefit, instead decreasing the SNR compared to single layer coils of approximately the same number of turns regardless of layer spacing to mitigate proximity effect. Importantly, the solid wire [19] and Litz wire [2] coils were tested at low detection frequencies and therefore utilized many turns *n*. Similar to *emf*, the conservative electric field E_C scales with $n \cdot B_0$ [21], with the result that low detection frequency coils maintain high electric fields. Consequently, multilayer coils were tested with a copper tape Faraday shield to ascertain whether the loss of SNR was an electric field phenomenon inducing undesirable currents in layers.

Table S3. Faraday shield results for square RF excitation pulses with 8 averages

Coil Reference	Coil Combination	Diameter (mm)	Length (mm)	Number of Turns	Q Factor	$\tau_{90°}$ (μs)	Noise (μVp-p)	NMR Signal (a.u.)
A	Inner	42	45	36	80	70	0.073	0.0739
B	Outer	51	45	36	52	118	0.049	0.0432
C	Inner+Outer	42/51	45	36+36	50	88	0.045	0.0588
D	Outer+Shield	51	45	36	36	142	0.055	0.0361
E	Inner+Outer+Shield	42/51	45	36+36	39	107	0.043	0.0478

The experimental setup for electric field testing involved two solenoids (Table S3) wound with 175/46 Litz wire. The phantom of 1.0 g of sodium 1-^{13}C-acetate was used with RF parameters of a square RF excitation pulse, 1 k complex points, 10 kHz spectral width, and 500 ms acquisition time for 8 signal averages. When tested in combination, the coils overlapped each other and used a series connection of the wire. The inner coil in isolation (A, Table S2) produced the highest signal. When tested in combination with the outer coil (C ⊥ A), despite the increased number of turns less NMR signal was detected. This decrease was in close accord with signal loss proportionate to Q loss, or 0.0584 projected signal according to $Signal_A \cdot \sqrt{Q_C/Q_A}$. Adding a Faraday shield between the coil and sample (D ⊥ B) decreased coil efficiency. Use of a shield between layers (E ⊥ C) also resulted in decreased coil efficiency. No combination of coils and shielding was found to improve coil sensitivity beyond that of the detection coil in isolation (A). For the conditions of the test, Faraday shields did not alleviate the loss of SNR that occurs with multilayer solenoid coils, indicating that the loss is not an *E*-field problem. In view of the previous multilayer tests [2, 19] and the solenoid microcoil theory [20], it appears from these tests that conductor thickness of Litz wire should be assessed on the overall bundle level rather than the strand level.

From the points mentioned above (Sections 3a – 3d), it is apparent that many variables must be balanced to achieve a RF coil that performs well. The inductance, resistance, number of turns, available space, and coil wind must all bear due consideration. The coil must conform closes to the sample to maximize signal, which has the additional benefit of minimizing the influence of coupling of the coil to the surrounding RF shield, gradient insert, or magnet bore. Generally one seeks to fulfill the formula of [minimizing resistance] while [maximizing inductance] while [maximizing turns], which can also be stated as [minimizing R] while [maximizing turn density]— something at which basket weaves excel. The MR sample itself must also be taken into consideration. For small animals, the interaction of detection frequency ω_0 with coil geometry and spatial constraints will typically result in too many turns and too little space, which prevents the use of parallel winds. For this situation the crystal radio coils represented by the basket weave form an optimal solution. On a larger scale as for human subjects, nearly the opposite set of constraints obtains: too few turns and a plenitude of space. In such situations, use of thicker wire and parallel winds become feasible means of increasing the SNR.

3. Experimental limitations and their SNR correction factors

Experimentally the SNR for prepolarized ^{1}H and ^{13}C at 0.0475 T was found to be almost identically 40% of the SNR available at 4.7 T. The theory presented in Eq. (S8) indicates that on the basis of frequency and coil efficiency differences alone, the detected signal should demonstrate at least equal sensitivity. In order to account for the sensitivity difference between theory and experiment, the sources of SNR gains and losses must be accounted for, which are inherent in the variables of Eq. (S8). The correction factors are presented in Table S4.

Table S4. Correction factors for $SNR_{0.0475T}/SNR_{4.7}$ gains and losses, Eq. (S8).

Source of SNR Loss (>1) & Gain (<1) (Factor)	^{1}H	^{13}C
~100 fold frequency difference	3.16	3.16
Coil coupling *Q* reduction	1.69	1.58
Litz R_C reduction (R_C*η_{Litz})	0.66	0.93
Utilized Litz stranding gauge G_S, Eq. (S19)	1.14	1.00
Deviation from optimal coil wire length	1.32	1.85
Increase in R_ST_S at 4.7 T, Eq. (S17)	0.78	0.91
Use of solenoid at 0.0475 T vs. saddle at 4.7 T	0.32	0.32
RF preamplifier noise figure	1.12	1.12
Proximity effect ζ	1.58	1.58
Coil temperature	1.03	1.03
Coil diameter	0.91	0.47
Predicted $SNR_{0.0475T}/SNR_{4.7T}$ (all factors included)	**0.45**	**0.46**
Experimental $SNR_{0.0475T}/SNR_{4.7T}$	**0.41**	**0.40**

The ^{1}H detection frequency ratio between the 4.7 T scanner and the 0.0475 T scanner was 200.24 MHz / 2.02 MHz, so that with the $\omega_0^{1/4}$ frequency dependence for hyperpolarized MR, Eq. (S8), ~100 fold frequency difference resulted in a 3.16 fold SNR loss. The ^{1}H detection 175/46 Litz wire had a calculated resistance reduction factor $\eta_{Litz} = 0.44$, and the ^{13}C 20/44 Litz wire $\eta_{Litz} = 0.86$, resulting in SNR gains of 0.66 and 0.93 respectively. The exact wave propagation velocity dependence for Litz wire constructions is not known, and was assumed to be that of bare copper wire, or factor $\alpha = 0.95$ times the speed of light. Given this velocity factor,

the optimal wire lengths for the 0.0475 T MR scanner resonant frequencies were ^{1}H = 14.10 m and ^{13}C = 56.07 m. The detection coils used 8.04 m and 16.43 m respectively. The solenoidal RF coil efficiency factor is 3.09^{-1} compared to a saddle coil. The 0.0475 T MR scanner system's narrow-band Miteq preamplifiers have a vendor specification of noise figure n_F = 0.5 dB. From perusal of commercial vendor information, a good preamplifier at high field has n_F = 0.4 dB, and a very good one n_F = 0.3 dB. n_F = 0.4 dB was used to account for the difference in scanner preamplifier noise figures. Other Table S4 factors are described in the following subsections.

3a. Coil coupling losses

Loss of Q due to close proximity to the RF shield was measured to account for coil coupling losses. An Agilent E5071C network analyzer was used to obtain the measurements. In the presence of the RF shield, the low field probes were tuned to the resonant frequencies of the 0.0475 T MR scanner and matched to -21 dB. The detection coil shielded Q measurements were Q_{1H} = 62.0 and Q_{13C} = 28.0. The RF shield was then removed and the probes re-tuned to the resonant frequencies and re-matched to -21 dB. The unshielded Q measurements were Q_{1H} = 196.0 and Q_{13C} = 77.3. As $SNR \propto \sqrt{Q}$ [2, 6] and Q losses from coupling should amount to no more than 10% [6], the coil coupling loss factors calculated as $\sqrt{0.9 \cdot Q_{unshielded} / Q_{shielded}}$ were 1.69 and 1.58 for ^{1}H and ^{13}C respectively (Table S4).

3b. Increase of 4.7 T $R_S T_S$ term

From Eqs. (S17) and (S18), the peak-to-peak noise measurements in Table S5 yield root-mean-square ratios $N_C/(N_C+N_S)$ leading to coil noise fractions of 0.76 and 0.92 for ^{1}H and ^{13}C respectively in Table S6. The coil resistance fractions in Table S5 demonstrate good agreement

between the two independent measurement methods. As Q measurements are more standard, these measurements were used for the coil noise fractions, which constitute the SNR gain factors.

Table S5. **Calculation of R_S loss factor and resulting R_C factor at 4.7 T**

Q Measurements			**Spectroscopic Noise Measurements**		
Value	**^{1}H**	**^{13}C**	**Value**	**^{1}H**	**^{13}C**
$\mathbf{Q_{Unloaded}}$	104	99.6	$\mathbf{N_S + N_C}$	40	94.8
$\mathbf{Q_{Loaded}}$	69	89.9	$\mathbf{N_C}$	23	80.5
$\mathbf{Q_L/Q_U}$	0.66	0.90	$\mathbf{N_C/(N_S+N_C)}$	0.58	0.85
$\mathbf{R_S = \% R_C}$	0.22	0.09	$\mathbf{R_S = \%R_C}$	0.24	0.13
$\mathbf{R_C = 1 - R_S}$	0.78	0.91	$\mathbf{R_C = 1 - R_S}$	0.76	0.87

3c. Stranding gauge effect

Litz wire stranding gauge selection implicates two potential sources of gains and losses— the effective Litz resistance reduction factor η_{Litz} directly and indirectly the length of wire l used in construction of the coil through interplay of Litz bundle diameter and coil geometry. For example, the experimental ^{1}H coils used a gauge less than ideal due to immediate commercial unavailability of the proper 48 AWG stranding gauge for ω_0 = 2.02 MHz. Thus, losses were increased over the optimal stranding gauge according to Eq. (S20) as

$$G_S = \left(\frac{l_{opt}\eta_{Litz,\ \exp}}{l_{\exp}\eta_{Litz,\ opt}} \right)^{1/2} . \qquad \text{(S20)}$$

As available through HM Wire International, 48 AWG stranding permits a 225 strand bundle with a 0.686 mm mean diameter, compared to the experimental 175 strands / 46 AWG of 0.737 mm mean diameter. The 225/48 conductor length used for the ^{1}H detection coil would have been l_{opt} = 9.29 m instead of $l_{\exp}$ = 8.04 m, and η_{Litz} would have been $\eta_{\text{Litz,opt}} = 0.41$ instead of $\eta_{\text{Litz,exp}} = 0.44$.

3d. Proximity effect calculation

As mentioned previously, proximity effect according to the Medhurst data depends upon two variables: the wire diameter-to-turn spacing ratio (d/s) and the coil length-to-coil diameter ratio (l_C/d_C). The detection coils had a (l_C/d_C) ratio of approximately 1.25. The proximity effect in the close wound condition (d/s) = 1 becomes worse for decreasing (l_C/d_C) ratio. Since it was estimated that approximately half the coil had (d/s) = 1 and the other (d/s) = 0.5, in order to avoid too favorable an accounting for proximity effect the Medhurst table entries for (l_C/d_C) = 2 were used instead of (l_C/d_C) = 1. For $\left(l_C/d_C\right)=2$ a fitting function to the (d/s) values yields the quartic polynomial

$$\zeta\left(\frac{d}{s}\right)=1.028-0.523\left(\frac{d}{s}\right)+6.806\left(\frac{d}{s}\right)^2-8.767\left(\frac{d}{s}\right)^3+5.565\left(\frac{d}{s}\right)^4 \qquad \text{(S21)}$$

$\zeta(1)$ = 4.11 and $\zeta(0.5)$ =1.72, yielding a total proximity effect for the detection coils of 2.50. An ideally spaced solenoid with 3 wire radii between centers [6] would have total proximity effect, Eq. (S21), of $\zeta(2/3)$ = 2.21.

To summarize, some SNR losses such as high preamplifier noise figure can be eliminated in low field, but proximity effect associated losses of multi-turn solenoid are unavoidable. When using optimal proximity effect of 1.31, Table S6 [22] for equally spaced wire for $\left(l_C/d_C\right)=2$

using optimal Litz wire with $\sqrt{R_C \cdot \eta_{Litz}}$ reduction by 0.66, 100-fold frequency ratio and use of solenoid vs. saddle RF coil geometry, it is indeed possible to achieve higher SNR in low field regime than that of high field, Table S6.

Table S6. Correction factors for SNR of optimal RF coil under conditions of ω_0(low field)=0.01*ω_0(high field)

Source of SNR Loss (>1) & Gain (<1) (Factor)	**Factor**
100 fold frequency difference	3.16
Litz R_C reduction in $\sqrt{R_C \cdot \eta_{Litz}}$	0.66
Use of solenoid at low field vs. saddle at high field	0.32
Proximity effect of multi-turn solenoid ζ	1.31
Theoretical $SNR_{low\ field}/SNR_{high\ field}$	**1.13**

References

[1] W. Dominguez-Viqueira, W. Berger, J. Parra-Robles, G.E. Santyr, Litz Wire Radiofrequency Receive Coils for Hyperpolarized Noble Gas MR Imaging of Rodent Lungs at 73.5 mT, Concept Magnetic Res. B, 37B (2010) 75-85.

[2] M.F. Carias, W. Dominguez-Viqueira, G.E. Santyr, Improving Signal-to-Noise Ratio of Hyperpolarized Noble Gas MR Imaging at 73.5 mT Using Multiturn Litz Wire Radiofrequency Receive Coils, Concept Magnetic Res. B, 39B (2011) 37-42.

[3] A.W. Lotfi, F.C. Lee, A high frequency model for Litz wire for switch-mode magnetics, in: Industry Applications Society Annual Meeting, Conference Record of the 1993 IEEE, 1993, pp. 1169-1175.

[4] K.M. Gilbert, T.J. Scholl, B.A. Chronik, RF coil loading measurements between 1 and 50 MHz to guide field-cycled MRI system design, Concept Magnetic Res. B, 33B (2008) 177-191.

[5] J. Mispelter, M. Lupu, A. Briguet, Nmr Probeheads for Biophysical And Biomedical Experiments: Theoretical Principles And Practical Guidelines, World Scientific Publishing Company, Incorporated, 2006.

[6] D.I. Hoult, R.E. Richards, The signal-to-noise ratio of the nuclear magnetic resonance experiment, J. Magn. Reson., 24 (1976) 71-85.

[7] K.R. Minard, R.A. Wind, Solenoidal microcoil design - Part II: Optimizing winding parameters for maximum signal-to-noise performance, Concept Magnetic Res., 13 (2001) 190-210.

[8] D.I. Hoult, P.C. Lauterbur, The sensitivity of the zeumatographic experiment involving human samples, J. Magn. Reson., 34 (1979) 425-433.

[9] B. Blasiak, V. Volotovskyy, C. Deng, B. Tomanek, An optimized solenoidal head radiofrequency coil for low-field magnetic resonance imaging, Magn. Reson. Imaging, 27 (2009) 1302-1308.

[10] K.R. Minard, R.A. Wind, Solenoidal microcoil design. Part I: Optimizing RF homogeneity and coil dimensions, Concept Magnetic Res., 13 (2001) 128–142.

[11] B.J.D. Marrocco, D.J. Drost, F.S. Prato, An optimized head coil design for MR imaging at 0.15-T, Magn. Reson. Med., 5 (1987) 143-159.

[12] C.P. Bidinosti, E.M. Chapple, M.E. Hayden, The sphere in a uniform RF field - Revisited, Concept Magnetic Res. B, 31B (2007) 191-202.

[13] D.G. Gadian, F.N.H. Robinson, Radiofrequency losses in NMR experiments on electrically conducting samples, J. Magn. Reson., 34 (1979) 449-455.

[14] T.W. Redpath, J.M.S. Hutchison, Estimating patient dielectric losses in NMR images, Magn. Reson. Imaging, 2 (1984) 295-300.

[15] F. Resmer, H.C. Seton, J.M.S. Hutchison, Cryogenic receive coil and low noise preamplifier for MRI at 0.01 T, J. Magn. Reson., 203 (2010) 57-65.

[16] P.L. Gor'kov, M. Wenping, J.A. Kitchen, I. Hung, M.W. Fey, W. Zhang, W.W. Brey, Solenoids revisited: improving performance of low-E detection coils, in: 53rd Annual ENC Conference, Miami, FL, 2012.

[17] A.H.M. Arnold, The Resistance of Round-Wire Single-Layer Inductance Coils, Proceedings of the IEE - Part IV: Institution Monographs, 98 (1951) 94.

[18] A.M. Coffey, R.V. Shchepin, K. Wilkens, K.W. Waddell, E.Y. Chekmenev, A Large Volume Double Channel 1H-X RF Probe for Hyperpolarized Magnetic Resonance at 0.0475 Tesla, J. Magn. Reson., 220 (2012) 94–101.

[19] R. Borowiak, N. Schwaderlapp, F. Huethe, T. Lickert, E. Fischer, S. Bär, J. Hennig, D. Elverfeldt, J.-B. Hövener, A battery-driven, low-field NMR unit for thermally and hyperpolarized samples, Magn. Reson. Mat. Phys. Biol. Med., (2013) 1-9.

[20] S.C. Grant, L.A. Murphy, R.L. Magin, G. Friedman, Analysis of multilayer radio frequency microcoils for nuclear magnetic resonance spectroscopy, IEEE Trans. Magn., 13 (2001) 2989-2998.

[21] P.L. Gor'kov, E.Y. Chekmenev, C.G. Li, M. Cotten, J.J. Buffy, N.J. Traaseth, G. Veglia, W.W. Brey, Using low-E resonators to reduce RF heating in biological samples for static solid-state NMR up to 900 MHz, J. Magn. Reson., 185 (2007) 77-93.

[22] R.G. Medhurst, H. F. Resistance and Self-Capacitance of Single-Layer Solenoids, Wireless Engineer, Feb. 35-43 (1947) Mar. 80-92.